

Maximum entropy temporal networks

Paolo Barucca

Department of Computer Science, University College London

Temporal networks consist of timestamped directed interactions rather than static links. These links may appear continuously in time, yet few studies have directly tackled the continuous-time modeling of networks. Here, we introduce a maximum entropy approach to temporal networks and with basic assumptions on constraints, the corresponding network ensembles admit a *modular* and *interpretable* representation: a set of global time processes—an inhomogeneous Poisson or a Hawkes process—and a static maximum-entropy (MaxEnt) edge, e.g. node pair, probability. This *time \times edge labels* factorization yields closed-form log-likelihoods, degree/unique-edge expectations, and yields a whole class of effective generative models. We provide *maximum-entropy derivation* of a log-linear Hawkes/NHPP intensity for temporal networks via functional optimization over path entropy, connecting inhomogeneous Poisson modeling -e.g. Hawkes models- to MaxEnt network ensembles. Global Hawkes time layers consistently improve log-likelihood over generic NHPP, while the MaxEnt edge labels recover strength constraints and reproduce expected unique-degree curves. We discuss the limitations of this unified framework and how it could be integrated with calibrated community/motif tools, Hawkes calibration procedures, and (neural) kernel estimation.

I. INTRODUCTION

Temporal networks -time-stamped interactions on a fixed or evolving node set-are a fundamental representation of social, economic, and biological systems. A central challenge in network theory is to build models that are *interpretable*, *principled*, and *predictive*. For static networks, maximum entropy ensembles have been introduced to account for degree/strength patterns, higher-order constraints [1–4], providing an ensemble of networks that is compatible with simple (explainable) network-level, community-level or, node-level quantities. On the other hand, the importance of principled clustering in networks via block models and mesoscale structure identification has been investigated in many works [5–8]. At the same time, self-exciting point processes originated in Hawkes’ seminal work, [9], have been shown to be an effective modeling assumption to reproduce burstiness and self-exciting behavior in a number of studies since [10–13]. The interaction between temporal covariances and Hawkes excitation has been leveraged for causal graph inference and clustering [14, 15]. Temporal networks have been studied in the literature [16, 17], to account for distinctive burstiness, memory, limited attention, and specific temporal patterns, e.g. temporal motifs. Recently, a maximum entropy approach has been introduced to model temporal networks in discrete time [17]. Despite the presence of advanced models for the calibration of multivariate Hawkes processes, [12, 14, 18], and for the modeling of static network ensembles, there is no principled maximum entropy model for temporal networks in continuous time. We here introduced a unified framework that combines the maximum-entropy (MaxEnt) principle for temporal network with the introduction of constraints on the point-process governing the event times. This approach provides an ensemble of temporal networks conditioned on a given set of simple constraints in the observed network quantities, whilst also providing a realistic set of timestamp patterns. The factorization that follows from

the maximum entropy approach allows us to (i) encode domain knowledge via linear constraints (e.g., strengths, unique edges, block structure) while (ii) capturing burstiness through a global Hawkes time process. We derive closed-form likelihoods, analytical expectations for unique degrees, and practical fitting routines (IPFP + bisection), and we validate the framework across diverse datasets (here presenting results on the Enron email dataset). Our contribution fills this gap by proposing a continuous-time maximum entropy approach that (i) defines the relevant entropy function for inhomogeneous Poisson processes adding a set of specific edge constraints (ii) block-mask constraints informed by clustering, and (iii) a clean decomposition of the likelihood between time and edge labels that simplifies estimation and comparison.

II. METHODOLOGY: MAXIMUM-ENTROPY TEMPORAL NETWORKS

Let $[0, T]$ be the observation window. A non-homogeneous Poisson process (NHPP) with intensity $\lambda(t) \geq 0$ is the point process for which: (i) the number of events on any set $A \subset [0, T]$ is Poisson with mean $\Lambda(A) := \int_A \lambda(t) dt$; and (ii) disjoint sets are independent. If $0 < t_1 < \dots < t_n < T$ are the observed times, the log-likelihood is

$$\log p(\{t_k\} | \lambda) = \sum_{k=1}^n \log \lambda(t_k) - \int_0^T \lambda(t) dt. \quad (1)$$

Taking expectation w.r.t. the same process and using Campbell’s theorem, $\mathbb{E} \sum_k f(t_k) = \int_0^T f(t) \lambda(t) dt$, yields the *negative expected log-likelihood* (a.k.a. *Poisson entropy functional*)

$$\mathcal{H}[\lambda] := -\mathbb{E}[\log p] = \int_0^T (\lambda(t) \log \lambda(t) - \lambda(t)) dt + \text{const.} \quad (2)$$

A. Maximum-entropy principle for temporal networks

We seek $\Lambda(t)$ that maximizes entropy subject to constraints related to sufficient statistics of interest. Throughout, we consider constraints of two types: (i) *structural/node/edge label* constraints that concern how mass is apportioned across edges (e.g., expected edge counts or node strengths), and (ii) *temporal* constraints that govern the global timeline (e.g., the inter-event kernel). We leverage the standard result that exponential-family models arise from maximum entropy with linear constraints.

B. Temporal networks as marked NHPPs

Consider a directed network with node set \mathcal{V} and edge set $\mathcal{E} \subseteq \mathcal{V} \times \mathcal{V}$. Each temporal event is a pair (t, m) with time $t \in [0, T]$ and mark $m = (i \rightarrow j) \in \mathcal{E}$. The model is a marked NHPP with edge-specific intensities $\lambda_{ij}(t) \geq 0$ and superposed (global) intensity $\Lambda(t) := \sum_{(i,j) \in \mathcal{E}} \lambda_{ij}(t)$. Denote the integrated intensities (“expected counts”) by

$$\mu_{ij} := \int_0^T \lambda_{ij}(t) dt. \quad (3)$$

C. Maximum entropy with linear constraints

We construct the maximum-entropy (MaxEnt) ensemble by minimizing $\sum_{ij} \mathcal{H}[\lambda_{ij}]$ subject to linear constraints

of two types: (i) *time-dependent* constraints on instantaneous totals; and (ii) *time-independent* constraints on the integrals (3). In addition to the per edge constraints, we use *node strengths* $s_i^{\text{out}} = \sum_j \mu_{ij}$ and $s_j^{\text{in}} = \sum_i \mu_{ij}$, and possibly *block-pair* totals $C_{ab} = \sum_{i \in a} \sum_{j \in b} \mu_{ij}$ for a node partition \mathcal{B} . For imposing constraints on admissible edges, including a potential block-structure, we introduce a binary *mask* $M_{ij} \in \{0, 1\}$ that encodes the allowed support $\mathcal{S} = \{(i, j) : M_{ij} = 1\}$ (*forbidden* edges have $\lambda_{ij} \equiv 0$).

Partitioned time-dependent constraints. Let $\mathcal{P} = \{E_r\}_{r=1}^R$ be a partition of edges ($E_r \cap E_{r'} = \emptyset$, $\cup_r E_r = \mathcal{E}$). For each part E_r we prescribe a target time profile $G_r(t) \geq 0$:

$$\sum_{(i,j) \in E_r} \lambda_{ij}(t) = G_r(t), \quad r = 1, \dots, R, \quad t \in [0, T]. \quad (4)$$

Special cases include a single global profile ($R = 1$, $G_1 = \Lambda$) or sender-specific profiles (take $E_r = \{(i, j) : i = r\}$).

D. Lagrangian and Euler-Lagrange equation

Introduce time-dependent multipliers $\alpha_r(t)$ for (4) and time-independent multipliers for mark-side constraints. The full Lagrangian is

$$\begin{aligned} \mathcal{L} = & - \sum_{(i,j) \in \mathcal{S}} \int_0^T (\lambda_{ij} \log \lambda_{ij} - \lambda_{ij}) dt \\ & + \sum_{r=1}^R \int_0^T \alpha_r(t) \left(\sum_{(i,j) \in E_r \cap \mathcal{S}} \lambda_{ij}(t) - G_r(t) \right) dt \\ & + \sum_{(i,j) \in \mathcal{S}} \Theta_{ij} \left(\int_0^T \lambda_{ij} dt - \mu_{ij}^* \right) + \sum_i \theta_i^{\text{out}} \left(\sum_j \int_0^T \lambda_{ij} dt - s_i^{\text{out},*} \right) \\ & + \sum_j \theta_j^{\text{in}} \left(\sum_i \int_0^T \lambda_{ij} dt - s_j^{\text{in},*} \right) + \sum_{a,b \in \mathcal{B}} \zeta_{ab} \left(\sum_{i \in a} \sum_{j \in b} \int_0^T \lambda_{ij} dt - C_{ab}^* \right). \end{aligned} \quad (5)$$

Stationarity w.r.t. $\lambda_{ij}(t)$ for $(i, j) \in \mathcal{S}$ and $r(i, j)$ the unique part with $(i, j) \in E_{r(i,j)}$ gives

$$\frac{\delta \mathcal{L}}{\delta \lambda_{ij}(t)} = -\log \lambda_{ij}(t) - 1 + \alpha_{r(i,j)}(t) + \Psi_{ij} = 0, \quad (6)$$

Where we grouped the Lagrangian multipliers into the log-linear *mark potential*

$$\Psi_{ij} = \Theta_{ij} + \theta_i^{\text{out}} + \theta_j^{\text{in}} + \zeta_{g(i),g(j)} + \log M_{ij}, \quad (7)$$

where any subset of terms can be used depending on the model (set absent multipliers to zero). Hence we derive the *multi-profile factorization*

$$\lambda_{ij}(t) = \phi_{r(i,j)}(t) w_{ij}, \quad \phi_r(t) := e^{\alpha_r(t)}, \quad w_{ij} := e^{\Psi_{ij}-1}. \quad (8)$$

Thus the MaxEnt solution always separates *time* and *marks*: each partition has its own time profile ϕ_r , while

all time-independent constraints determine the weights w_{ij} .

E. Enforcing the constraints

Define $W_r := \sum_{(i,j) \in E_r \cap \mathcal{S}} w_{ij}$ and $\Lambda_r := \int_0^T \phi_r(t) dt$. The partition constraints (4) imply

$$\phi_r(t) = \frac{G_r(t)}{W_r}, \quad r = 1, \dots, R. \quad (9)$$

Time-independent constraints act on the integrals:

$$\mu_{ij} = \int_0^T \lambda_{ij}(t) dt = \Lambda_{r(i,j)} w_{ij}, \quad (10)$$

together with chosen margins (edge totals, strengths, block totals). In practice, (10) reduces to *masked biproportional scaling* (IPF/Sinkhorn) on w_{ij} , optionally with block factors, exactly as in static MaxEnt ensembles.

F. Notable cases

All models are cases of (8); they differ only by the constraints that are active.

(1) *Edge-Poisson (edge totals only)*. No time constraint; $\int \lambda_{ij} = \mu_{ij}^*$.

$$\lambda_{ij}(t) \equiv \mu_{ij}^*/T. \quad (11)$$

(2) *Global Hawkes + edge totals*. Single time profile ($R = 1$) constrained to a fitted global Hawkes intensity $\lambda_H(t)$. With $S = \sum_{ij} \mu_{ij}^*$ and $\Lambda_H = \int_0^T \lambda_H dt$,

$$\lambda_{ij}(t) = \frac{\mu_{ij}^*}{\Lambda_H} \lambda_H(t) \quad (\phi(t) = \frac{S}{\Lambda_H} \lambda_H(t), w_{ij} = \mu_{ij}^*/S). \quad (12)$$

(3) *Global Hawkes + strengths + mask*. Constraints: $\sum_{ij} \lambda_{ij}(t) = \lambda_H(t)$; strengths $s_i^{\text{out},*}$, $s_j^{\text{in},*}$; mask M_{ij} . Then

$$\lambda_{ij}(t) = \phi(t) x_i y_j M_{ij}, \quad (13)$$

$$\sum_j x_i y_j M_{ij} = \frac{s_i^{\text{out},*}}{\int \phi dt}, \quad \sum_i x_i y_j M_{ij} = \frac{s_j^{\text{in},*}}{\int \phi dt}. \quad (14)$$

This model is the temporal equivalent of the Directed Weighted Configuration Model (DWCM), [3], with timestamps assigned by the fitted Hawkes process.

(4) *Global Hawkes + strengths + block-degree constraints via mask (unique edges)*. Constraints on *number of distinct edges* between blocks by encoding them in the mask. Let $g: \mathcal{V} \rightarrow \mathcal{B}$ be the block map and let $K_{ab}^* \in \mathbb{N}$ be the target number of unique edges from block a to block b . Choose subsets

$$\mathcal{S}_{ab} \subseteq \{(i, j) : g(i) = a, g(j) = b\}, \quad |\mathcal{S}_{ab}| = K_{ab}^*,$$

and define the block-degree mask,

$$M_{ij} = \begin{cases} 1, & (i, j) \in \mathcal{S}_{ab} \text{ with } g(i) = a, g(j) = b, \\ 0, & \text{otherwise,} \end{cases} \quad (15)$$

$$\sum_{i \in a} \sum_{j \in b} M_{ij} = K_{ab}^* \quad \forall a, b. \quad (16)$$

With $\sum_{ij} \lambda_{ij}(t) = \lambda_H(t)$ and strengths as in (3), the model is

$$\lambda_{ij}(t) = \phi(t) x_i y_j M_{ij}, \quad \phi(t) = \frac{S}{\Lambda_H} \lambda_H(t), \quad (17)$$

$$\sum_j x_i y_j M_{ij} = \frac{s_i^{\text{out},*}}{\int \phi dt}, \quad \sum_i x_i y_j M_{ij} = \frac{s_j^{\text{in},*}}{\int \phi dt}, \quad (18)$$

i.e., a DWCM on a fixed, block-degree-constrained support that enforces exactly K_{ab}^* unique edges per block pair, with timestamps assigned by the Hawkes profile ϕ . In practice, \mathcal{S}_{ab} can be taken from training data (e.g., the K_{ab}^* most active dyads) or selected by a small matching/covering heuristic; once M is fixed, the MaxEnt problem remains convex.

(5) *Sender-specific (outgoing-links) Hawkes + strengths + mask*. Partition by sender: $E_r = \{(i, j) : i = r\}$ and set $G_r(t) = \phi_i(t) = c_i \lambda_i^H(t)$ from a univariate Hawkes fit on sender events. Then

$$\lambda_{ij}(t) = \phi_i(t) w_{ij}^{(i)} M_{ij}, \quad \sum_j w_{ij}^{(i)} = 1 \text{ on } \mathcal{S}, \quad (19)$$

and strengths fix the remaining margins.

(6) *Partitioned time constraints + (optional) strengths/block totals*. For a general edge partition \mathcal{P} with targets $G_r(t)$,

$$\lambda_{ij}(t) = \phi_{r(i,j)}(t) w_{ij}, \quad \phi_r(t) = \frac{G_r(t)}{\sum_{(i,j) \in E_r} w_{ij}}, \quad (20)$$

and w_{ij} is calibrated to match the selected time-independent margins on the mask.

G. Estimating and generating data

Constraint compatibility requires: (i) $\int_0^T G_r dt = S_r$ (by construction here); (ii) strength/block margins sum to S and agree across decompositions; (iii) the mask \mathcal{S} admits a feasible nonnegative w with the requested margins (checked via masked IPF or max-flow diagnostics). Under these conditions, the intensities $\{\lambda_{ij}(t)\}$ are measurable, nonnegative, and integrable; superposition $\sum_{ij} \lambda_{ij}(t) = \sum_r G_r(t)$ stays finite and the model defines a valid marked NHPP. Sampling is straightforward: for each part r simulate an NHPP with rate $G_r(t)$; at each event time, draw the mark within E_r with probabilities $\{w_{ij}\}_{(i,j) \in E_r}$, showing how the maximum entropy approach recovers, yet generalising, the shuffling methodologies that are generally utilised as a simple benchmark.

III. RESULTS

We now present the empirical results obtained on the Enron dataset using the Maximum Entropy Temporal Network (METN) framework and its variants. The results are divided into three main parts: inter-event time distributions, network properties (degree, clustering, motifs), and combined properties including log-likelihood evaluation, raster plots, top-nodes raster plots, and block raster plots.

A. Inter-event time distribution

We begin with the analysis of the inter-event time distribution. Figure 1 compares the empirical distribution of inter-event times with the exponential distribution corresponding to a homogeneous Poisson process fitted at the empirical rate. The empirical distribution exhibits clear deviations from the exponential benchmark, showing a heavy concentration at very short timescales. This indicates the presence of bursty dynamics, which are not captured by the homogeneous Poisson model.

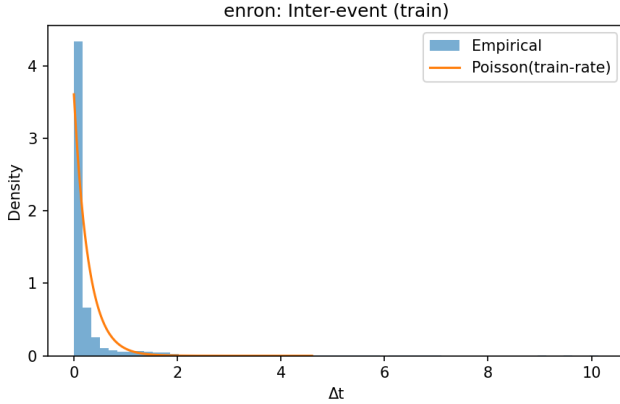


FIG. 1: Inter-event time distribution for Enron (train). The empirical density is shown alongside the exponential distribution with the same average rate.

Table I reports empirical mean/variance of inter-event gaps per split and the corresponding values implied by Poisson and Hawkes. For Hawkes with branching ratio $\eta < 1$ and exogenous rate μ , the mean stationary rate is $\bar{\lambda} = \mu/(1 - \eta)$ so $\mathbb{E}[\Delta t] \approx 1/\bar{\lambda}$ (variance depends on kernel; both exponential and power-law kernels yield overdispersion relative to Poisson).

B. Network properties

Next, we focus on the structural properties of the network.

a. Degree and clustering. The scatterplots in Figures 3–2 show the relationship between expected clustering coefficients and expected degrees for three generative models (BlockMask, EdgePoisson, MEstrength) as well as the empirical network. The BlockMask (Figure 3) is able to reproduce clustering for low-degree nodes more accurately compared to EdgePoisson (Figure 4), while MEstrength (Figure 5) produces a broader spread of clustering values but deviates significantly at higher degrees. The empirical distribution (Figure 2) reveals the characteristic decay of clustering with degree.

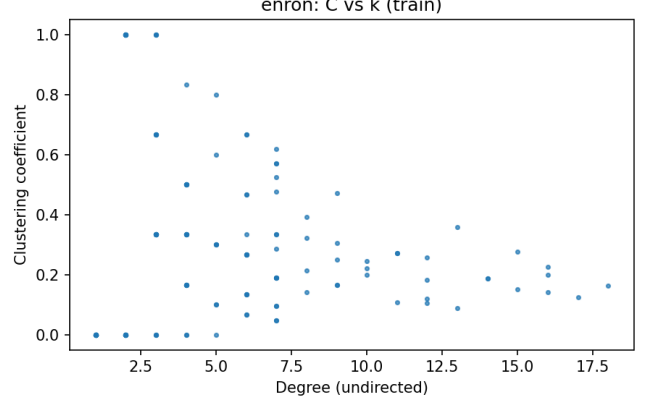


FIG. 2: Empirical clustering vs. degree for Enron (train).

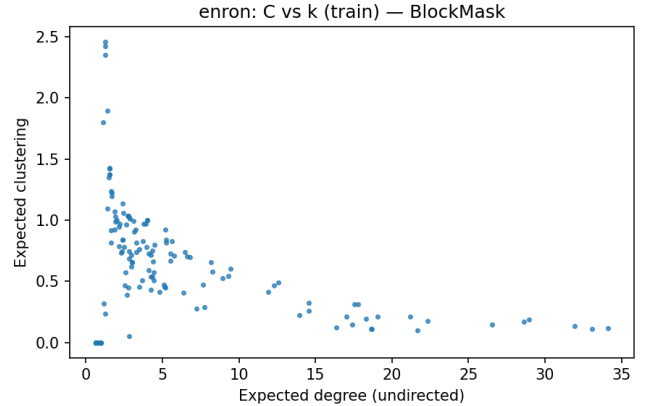


FIG. 3: Expected clustering vs. degree for BlockMask model on Enron (train).

b. Degree calibration. Figure 6 shows the calibration of the ME model in terms of expected versus empirical out-degree. The agreement is very good across the distribution, except for a few extreme nodes with very high degree.

Table II compares observed unique directed links on train/test with model expectations from Edge-Poisson (EP), ME-Strength (ME), and Block-Mask (BM). Expectations follow $\mathbb{E}[U_{\rightarrow}] = \sum_{i \neq j} (1 - e^{-\mu_{ij}})$ under Poissonization with K events. BM typically narrows the gap

TABLE I: Inter-event statistics by split. Poisson uses train-rate on train and split MLE otherwise; Hawkes parameters are fit per split.

Dataset	Split	$\mathbb{E}[\Delta t]$ (emp)	$\text{Var}[\Delta t]$ (emp)	$K - 1$	$1/\hat{\lambda}$	$1/\hat{\lambda}^2$	HawkesExp mean	HawkesExp var	HawkesPL mean	HawkesPL var
enron	train	0.277	0.576	2,999	0.277	0.077	0.290	0.536	0.493	0.606
enron	test	0.169	0.284	999	0.277	0.077	0.172	0.289	0.213	0.284

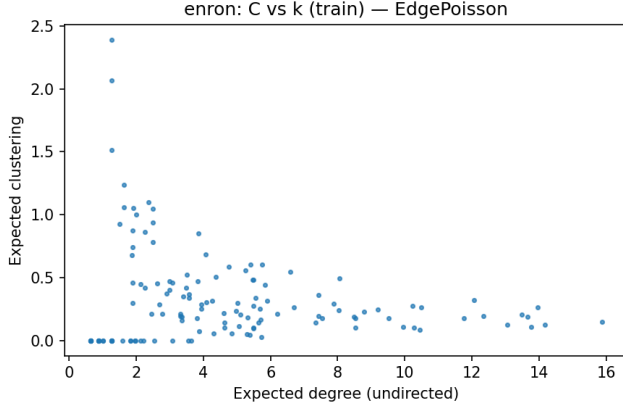


FIG. 4: Expected clustering vs. degree for EdgePoisson model on Enron (train).

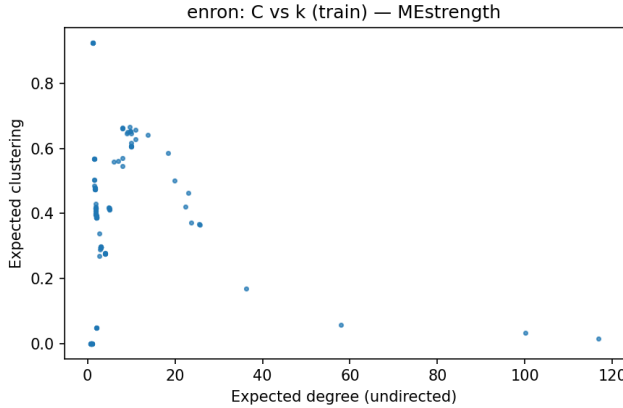


FIG. 5: Expected clustering vs. degree for MEstrength model on Enron (train).

Δ by allocating probability mass within communities; ME aligns rows/columns with node strengths but may under-cover unseen pairs if the mask is too tight; EP spreads mass proportional to counts.

c. Motif statistics. Figures 7–9 report the rates of four key directed motifs (reciprocity, broadcast, convergence, repeat) normalized by opportunities. The empirical baseline (Figure 9) shows the observed motifs in the dataset. The HawkesExp model (Figure 7) strongly amplifies broadcast and convergence motifs, capturing bursty group communications, while EdgePoisson underestimates reciprocity. The Poisson baseline (Figure 8)

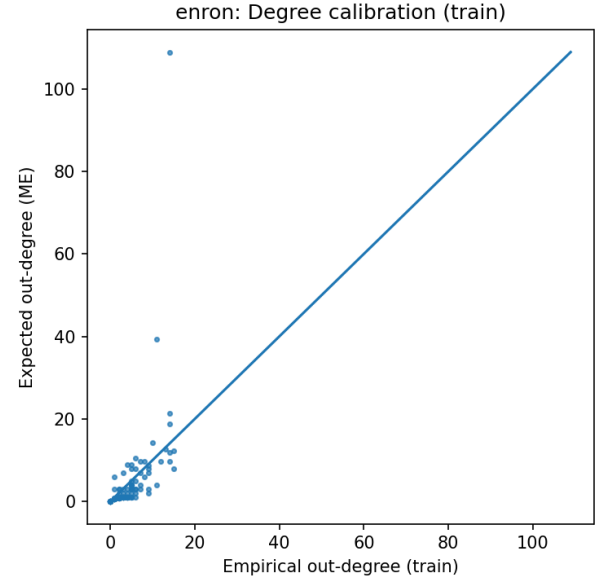


FIG. 6: Calibration of out-degree: expected (ME) vs. empirical for Enron (train).

shows weaker deviations, highlighting the importance of temporal correlations in motif amplification.

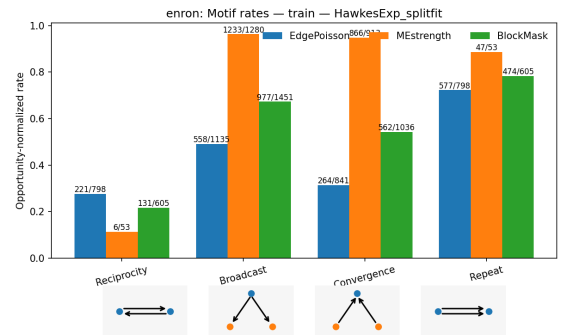


FIG. 7: Motif occurrence rates for Enron (train), HawkesExp splitfit compared with maximum entropy baselines.

TABLE II: Edge coverage and expected unique directed links (train/test). Expected values use $\mathbb{E}[U_{\rightarrow}] = \sum_{i \neq j} (1 - e^{-\mu_{ij}})$.

Dataset	n	K_{train}	K_{test}	$U_{\rightarrow}^{\text{obs}}(\text{train})$	$U_{\rightarrow}^{\text{obs}}(\text{test})$	$\mathbb{E}_{\text{EP}}[U_{\rightarrow}](\text{train})$	$\mathbb{E}_{\text{EP}}[U_{\rightarrow}](\text{test})$	$\mathbb{E}_{\text{ME}}[U_{\rightarrow}](\text{train})$	$\mathbb{E}_{\text{ME}}[U_{\rightarrow}](\text{test})$	$\mathbb{E}_{\text{BM}}[U_{\rightarrow}](\text{train})$	$\mathbb{E}_{\text{BM}}[U_{\rightarrow}](\text{test})$
enron	142	3,000	1,000	513	302	414.02	268.60	514.02	401.55	501.03	340.21

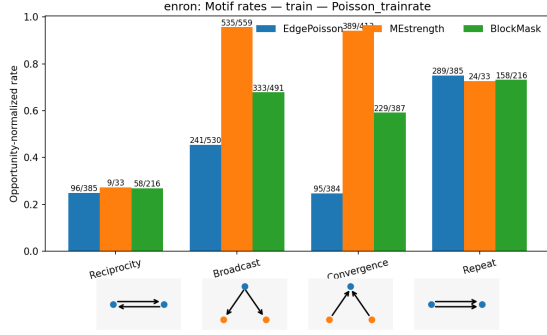


FIG. 8: Motif occurrence rates for Enron (train), Poisson baseline compared with maximum entropy baselines.

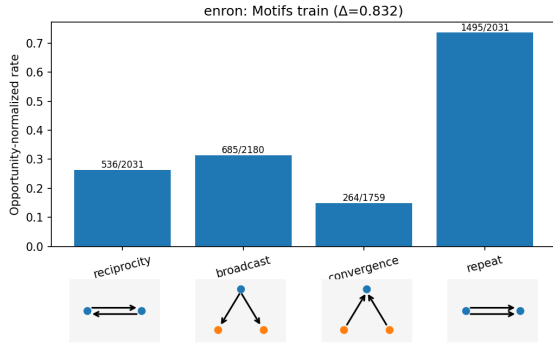


FIG. 9: Empirical motif occurrence rates for Enron (train).

C. Combined properties, likelihoods, and raster plots

We further explore combined temporal-structural properties using raster plots and likelihood analysis. Figures 10 and 11 report per-event log-likelihoods for the mark and temporal components respectively. The mark likelihoods (Figure 10) highlight that EdgePoisson best explains edge selection, while MEStrength struggles. In contrast, the temporal likelihoods (Figure 11) showing the higher likelihood of Hawkes processes over Poisson baselines, capturing the burstiness of event timings, yet not demonstrating their statistical significance as no model selection is here performed.

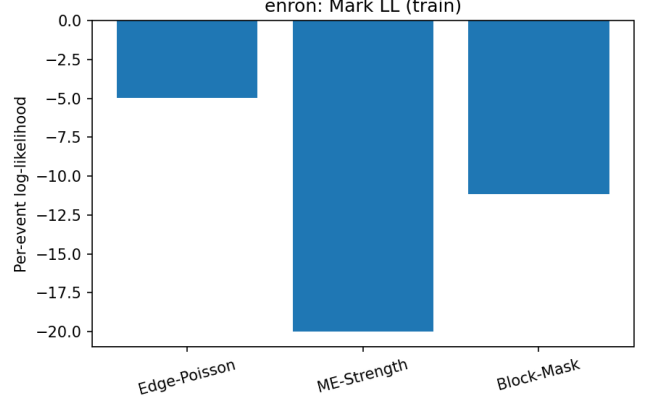


FIG. 10: Per-event mark log-likelihood for Enron (train) across models.

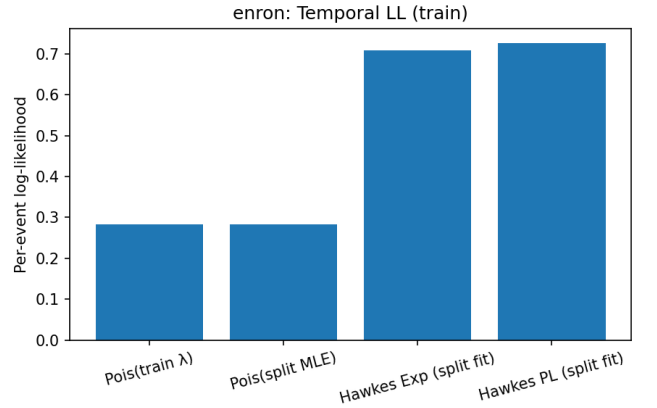


FIG. 11: Per-event temporal log-likelihood for Enron (train). Hawkes models clearly outperform Poisson baselines.

Figures 12–15 show the outgoing and incoming communication patterns of the top-10 nodes. The empirical raster (Figure 12) exhibits heterogeneous bursty patterns, which are only partially reproduced by the models. Among them, the HawkesExp \times BlockMask (Figure 13) shows the closest match, while EdgePoisson (Figure 14) and MEStrength (Figure 15) fail to capture the density and clustering of bursts.

Similarly, block-level raster plots (Figures 16–18) provide a mesoscopic view of temporal activity. The empirical block raster (Figure 16) reveals heterogeneous burst structures across groups, which are best captured by HawkesExp \times BlockMask (Figure 17). The Poisson baseline

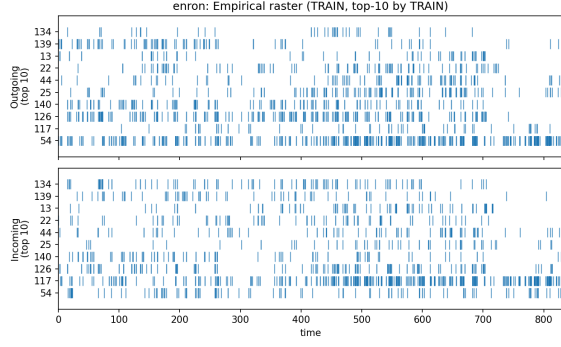


FIG. 12: Empirical raster plot for top-10 nodes by activity (Enron, train).

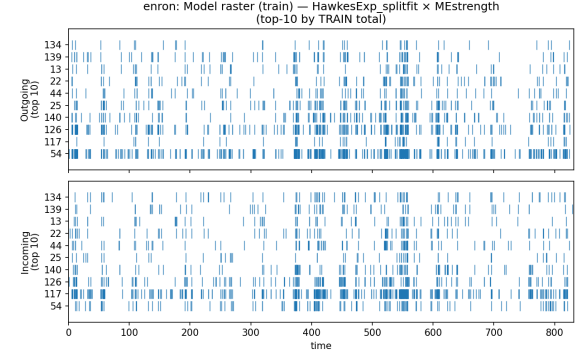


FIG. 15: Model raster plot: HawkesExp \times MEstrength (Enron, train).

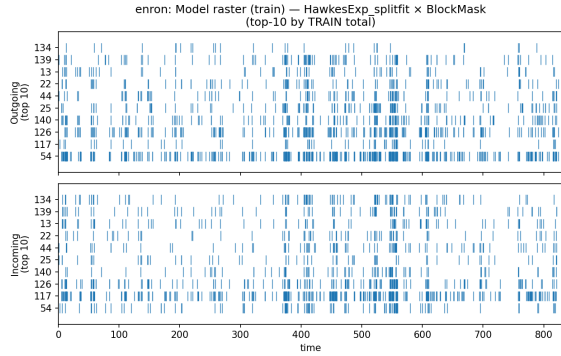


FIG. 13: Model raster plot: HawkesExp \times BlockMask (Enron, train).

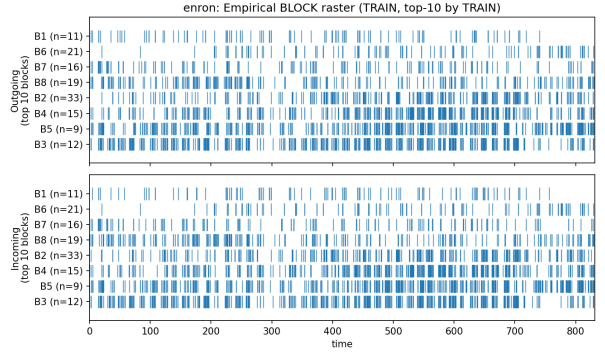


FIG. 16: Empirical block raster (top-10 blocks, Enron, train).

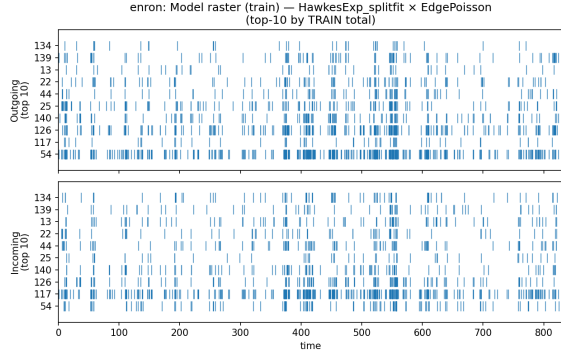


FIG. 14: Model raster plot: HawkesExp \times EdgePoisson (Enron, train).

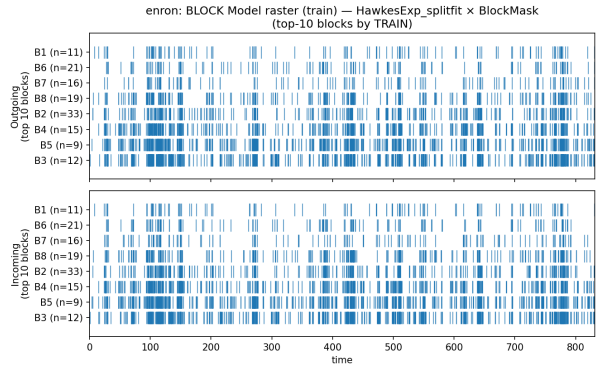


FIG. 17: Block raster: HawkesExp \times BlockMask (Enron, train).

(Figure 18) shows nearly uniform densities, missing the heterogeneity of burst patterns.

IV. CONCLUSIONS

This study has introduced a generalised maximum entropy approach for temporal networks in continuous time.

Our results confirm that purely static maximum entropy models (EdgePoisson, MEstrength, BlockMask) reproduce degree and clustering constraints but generally tend to fail to match higher-order temporal features. The addition of Hawkes-type self-excitation improves the match with empirical inter-event times, motif statistics, raster plot heterogeneity, and temporal likelihoods, pointing to

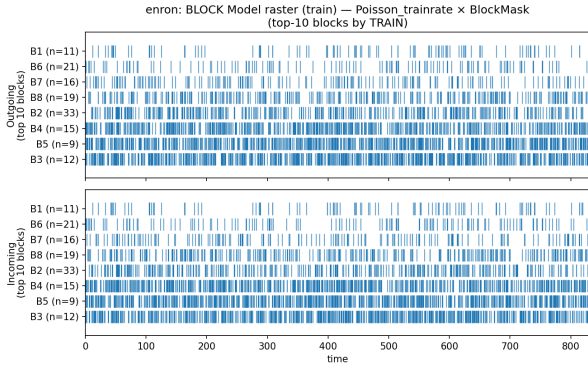


FIG. 18: Block raster: Poisson baseline \times BlockMask (Enron, train).

the fundamental role of bursty dynamics in shaping temporal networks. This unified framework, which we have shown to be effective in estimating and generating networks from the ensembles here introduced, does not solve the general problem of the optimal edge classification for the full multivariate point-process estimation of the whole temporal network model. Nevertheless, it provides a clear set of temporal network models that can integrate the intensities estimated from fully fledged multivariate point-process models, and it could serve as a solid framework to test and integrate Hawkes calibration procedures [14], higher-order network properties, neural kernel estimation methods, and graph neural network models.

-
- [1] E. T. Jaynes, *Physical Review* **106**, 620 (1957).
 - [2] I. Csizsár, *The Annals of Probability* **3**, 146 (1975).
 - [3] G. Cimini, T. Squartini, F. Saracco, D. Garlaschelli, A. Gabrielli, and G. Caldarelli, *Nature Reviews Physics* **1**, 58 (2019).
 - [4] M. Newman, *Networks* (Oxford University Press, 2018).
 - [5] B. Karrer and M. E. J. Newman, *Physical Review E* **83**, 016107 (2011).
 - [6] K. Rohe, T. Qin, and B. Yu, *Proceedings of the National Academy of Sciences* **113**, 12679 (2016).
 - [7] D. L. Sussman, M. Tang, and C. E. Priebe, *Universally consistent latent position estimation and vertex classification for random dot product graphs* (2012), [arXiv:1207.6745 \[stat.ML\]](#).
 - [8] M. E. J. Newman, *Proceedings of the National Academy of Sciences* **98**, 404 (2001).
 - [9] A. G. Hawkes, *Biometrika* **58**, 83 (1971).
 - [10] Y. Ogata, *Journal of the American Statistical Association* **83**, 9 (1988).
 - [11] E. Bacry, I. Mastromatteo, and J.-F. Muzy, *Market Microstructure and Liquidity* **1**, 1550005 (2015).
 - [12] E. Bacry and J.-F. Muzy, *IEEE Transactions on Information Theory* **62**, 2184 (2016).
 - [13] V. Filimonov and D. Sornette, *Physical Review E—Statistical, Nonlinear, and Soft Matter Physics* **85**, 056108 (2012).
 - [14] M. Achab, E. Bacry, S. Gaïffas, I. Mastromatteo, and J.-F. Muzy, *Journal of Machine Learning Research* **18**, 1 (2017).
 - [15] L. Mercuri, A. Perchiazzo, and E. Rroji, *Insurance: Mathematics and Economics* **116**, 1 (2024).
 - [16] N. Masuda and R. Lambiotte, *A Guide to Temporal Networks*, Complexity Science, Vol. 4 (World Scientific, Singapore, 2016).
 - [17] G. V. Clemente, C. J. Tessone, and D. Garlaschelli, *arXiv preprint arXiv:2311.16981* (2023).
 - [18] H. Soliman, L. Zhao, Z. Huang, S. Paul, and K. S. Xu, in *Proceedings of the 39th International Conference on Machine Learning*, Proceedings of Machine Learning Research, Vol. 162 (PMLR, 2022) pp. 20329–20346.

V. APPENDIX

A. Time-marks separation for the log-likelihood

For observed events $\{(t_k, m_k)\}_{k=1}^n$ with marks $m_k = (i_k \rightarrow j_k)$ and edge-wise counts N_{ij} , the marked NHPP log-likelihood is

$$\ell(\{\lambda_{ij}\}) = \sum_{k=1}^n \log \lambda_{i_k j_k}(t_k) - \sum_{(i,j)} \int_0^T \lambda_{ij}(t) dt. \quad (21)$$

In all models below the MaxEnt solution factorizes either *globally* as

$$\lambda_{ij}(t) = \phi(t) w_{ij}, \quad W := \sum_{i,j} w_{ij}, \quad (22)$$

or by partition $\mathcal{P} = \{E_r\}_{r=1}^R$ as

$$\lambda_{ij}(t) = \phi_{r(i,j)}(t) w_{ij}, \quad W_r := \sum_{(i,j) \in E_r} w_{ij}. \quad (23)$$

Plugging (22) into (21) gives

$$\ell(\phi, w) = \underbrace{\sum_{k=1}^n \log \phi(t_k) - W \int_0^T \phi(t) dt}_{\ell_{\text{time}}(\phi; W)} + \underbrace{\sum_{i,j} N_{ij} \log w_{ij}}_{\ell_{\text{mark}}(w)}. \quad (24)$$

Likewise, under (23)

$$\ell(\{\phi_r\}, w) = \sum_{r=1}^R \left[\sum_{k: m_k \in E_r} \log \phi_r(t_k) - W_r \int_0^T \phi_r(t) dt \right] + \sum_{i,j} N_{ij} \log w_{ij}. \quad (25)$$

B. Block–block verification (train).

We compare observed unique directed edges per (a, b) with the Block-Mask expectation 19.

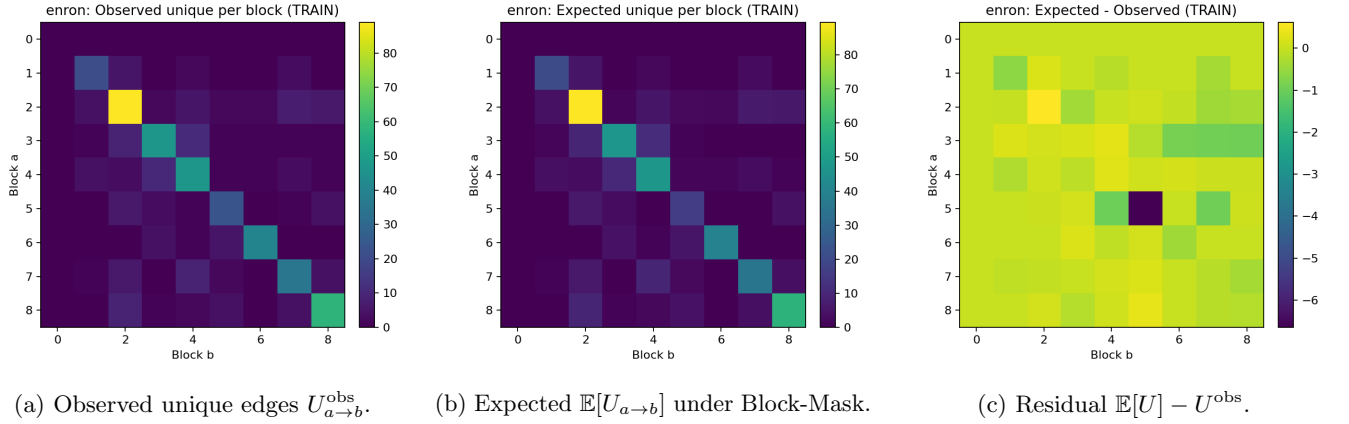


FIG. 19: **Block–block unique-edge calibration (train).** Diagonals (within-block) dominate. Small residuals indicate that the tuned quotas M_{ab} with IPFP reproduce TRAIN-level unique-link structure; large negative cells flag underfit block pairs.